Original Article

Identification of a ferroptosis-related gene signature for the prognosis of pediatric neuroblastoma

Xijin Lin[1]^, Kongfeng Shao[1], Zhuangbin Lin[2], Qiandong Liang[1], Xiaoyan Li[1], Haiyan Chen[3], Junxin Wu[1,4]

[1]Department of Radiation Oncology, Fujian Children's Hospital (Fujian Branch of Shanghai Children's Medical Center), College of Clinical Medicine for Obstetrics & Gynecology and Pediatrics, Fujian Medical University, Fuzhou, China; [2]Department of Radiation Oncology, Fujian Medical University Union Hospital, Fuzhou, China; [3]Department of Radiation Oncology, Renji Hospital, Shanghai Jiao Tong University School of Medicine, Shanghai, China; [4]Department of Radiation Oncology, Fujian Medical University Cancer Hospital, Fujian Cancer Hospital, Fuzhou, China

Contributions: (I) Conception and design: X Lin, J Wu; (II) Administrative support: Q Liang, X Li; (III) Provision of study materials or patients: Q Liang, X Li; (IV) Collection and assembly of data: X Lin, Z Lin, K Shao; (V) Data analysis and interpretation: X Lin, H Chen, J Wu; (VI) Manuscript writing: All authors; (VII) Final approval of manuscript: All authors.

Correspondence to: Junxin Wu, MD, PhD. Department of Radiation Oncology, Fujian Children's Hospital (Fujian Branch of Shanghai Children's Medical Center), College of Clinical Medicine for Obstetrics & Gynecology and Pediatrics, Fujian Medical University, Fuzhou 350005, China; Department of Radiation Oncology, Fujian Medical University Cancer Hospital, Fujian Cancer Hospital, 420 Fuma Rd, Jin'an District, Fuzhou 350014, China. Email: junxinwufj@aliyun.com; Haiyan Chen, MD, PhD. Department of Radiation Oncology, Renji Hospital, Shanghai Jiao Tong University School of Medicine, 227 South Chongqing Road, Shanghai 200025, China. Email: chenhaiyan1220@163.com.

Background: Ferroptosis-related genes are correlated with the prognosis of patients with neuroblastoma (NB) remains unknown. This study aims to establish a prognostic ferroptosis-related gene model for predicting prognostic value in pediatric NB patients.

Methods: The gene expression array and clinical characteristics of NB were downloaded from a public database. Correlations between ferroptosis-related genes and drug responses were analyzed by Childhood Cancer Therapeutics. The prognostic model was constructed by least absolute shrinkage and selection operator (LASSO) Cox regression and was validated in NB patients from the ICGC cohort. The survival analysis was performed by Cox regression analysis. single-sample gene set enrichment analysis (ssGSEA) was used to quantify the immune cell infiltration correlation.

Results: Overall, 70 genes were identified as ferroptosis-related differentially expressed genes (DEGs) from 247 samples. Then, 13 ferroptosis-related genes were correlated with OS in the univariate Cox regression analysis. Five prognostic ferroptosis-related DEGs (pFR-DEGs) (*STEAP3*, *MAP1LC3A*, *ULK2*, *MTOR* and *TUBE1*), which were defined as the intersection of DEGs and prognostic ferroptosis-related genes, were identified and utilized to construct the prognostic signature. The correlation between five pFR-DEGs and drug responses was analyzed, and the box plots indicated that *MTOR* gene expression was highest, suggesting that *MTOR* expression is related to progressive NB disease. The receiver operating characteristic (ROC) curve showed that the model had moderate predictive power. The survival analysis indicated that the high-risk group had poor overall survival (OS) ($P=2.087\times10^{-06}$). Univariate and multivariate analyses identified the risk score as a significant prognostic risk factor [P=0.003, hazard ratio (HR) =1.933]. Immune cell infiltration correlation analysis showed that the high-risk group was related to more immune cells.

Conclusions: The present study indicated a difference in ferroptosis-related gene expression between low- and high-risk NB patients. The ferroptosis-related signature could serve as a prognostic prediction tool. Additionally, immune infiltration might play an important role in different risk groups for NB patients.

Keywords: Pediatric neuroblastoma; ferroptosis-related gene; signature; prognosis; immune cells

^ ORCID: 0000-0001-8140-8187.

Submitted Feb 20, 2024. Accepted for publication May 24, 2024. This article was updated on September 19, 2024.
The original version is available at: https://dx.doi.org/10.21037/tcr-24-269
doi: 10.21037/tcr-24-269

Introduction

Neuroblastoma (NB) is the most common extracranial solid tumor in infants and children (1,2), and the mortality rate of NB is the third highest, behind leukemia and brain tumors (2,3). The prognosis of patients with NB varies widely. Through the NB risk classification system from the Children's Oncology Group (COG), the patients were divided into low-, intermediate- and high-risk groups (4). Over the past decades, despite intensive treatment, the survival rates for high-risk children remain poor, with a 5-year survival rate of 40–50% (2,3,5-8). The main treatment of NB is still in the form of multidisciplinary combination. The COG protocol (A3961) showed that patients with intermediate-risk NB who received chemotherapy of cyclophosphamide, doxorubicin, carboplatin, and etoposide had a 96% 3-year overall survival (OS) (9). In high-risk NB, intensive chemotherapy is one of the important approaches using a carboplatin/etoposide/melphalan preparative regimen according to the COG high-risk neuroblastoma protocol (ANBL 0532) (10). The biology and genetic basis of NB are currently being studied, and the combination may be an advantageous therapeutic approach. Therefore, considering the possibility of genetic-related therapy for NB, there is an additional need for the development of prognostic models.

Ferroptosis is a new nonapoptotic modality of cell death that is iron-dependent and driven by the production of lipid reactive oxygen species (ROS) (11-13). Ferroptosis differs from apoptosis, pyroptosis, autophagy and other forms of regulated cell death (14-16). Ferroptosis could not be inhibited by the traditional inhibitors of apoptosis, pyroptosis and autophagy (17). The main factors contributing to ferroptosis were the iron metabolism disruption, the production of free radical, the suppletion of fatty acid and lipid peroxidation (18) and the ferroptosis could be inhibited by iron chelators, antioxidant (13,17). In recent years, because of the higher levels of iron in neoplasms (19), ferroptosis has played an important role in the occurrence and development of related tumors, including pancreatic cancer, hepatocellular carcinoma, breast cancer, and gastric cancer (20-24). A previous study revealed that ferroptosis is an anticancer strategy in NB using withaferin A, an anticancer agent (25). Geng *et al.* found that knocking down ferroprotein, the sole iron export protein, can accelerate ferroptosis (26). Similarly, some researchers indicated that, because of inadequate ferritin heavy chain (Fth), ferroptosis cell death results in NB cells induced by erastin or RSL3 (27). Above all, studies have provided evidence that ferroptosis genes might be new therapeutic targets in NB. However, whether these ferroptosis-related genes are correlated with the prognosis of patients with NB remains unknown. Therefore, there is an urgent need to analyze ferroptosis-related genes to improve NB patient outcomes.

In the present study, the gene expression data and clinical characteristics in NB from the Therapeutically Applicable Research to Generate Effective Treatments (TARGET) were analyzed, and ferroptosis-related differentially expressed genes (DEGs) were used to construct a prognostic multigene signature and explore the underlying mechanism. We present this article in accordance with the TRIPOD

Highlight box

Key findings

- The present study indicated a difference in ferroptosis-related gene expression between low- and high-risk neuroblastoma (NB).
- The expression of *MTOR* gene is related to progressive NB.
- Immune infiltration might play an important role in different risk groups for NB patients.

What is known and what is new?

- Ferroptosis is a new nonapoptotic modality of cell death which has played an important role in the occurrence and development of tumors.
- The novel signature constructed by ferroptosis-related genes and the risk score model might be helpful for predicting prognosis and could improve immunotherapy.

What is the implication, and what should change now?

- The ferroptosis-related signature could serve as a prognostic prediction tool.
- More experimental and clinical data are needed to confirm the risk signature and the gene signature.

Table 1 Clinical characteristics of the NB patients

Characteristic	TARGET	ICGC
Gender, n (%)		
Male	143 (57.4)	629 (56.9)
Female	106 (42.6)	476 (43.1)
Age (years), n (%)		
≤5	228 (91.6)	1,005 (91.0)
>5	21 (8.4)	100 (9.0)
INSS stage, n (%)		
Stage 1	30 (12)	90 (8.1)
Stage 2	0 (0)	61 (5.5)
Stage 3	1 (0.4)	92 (8.3)
Stage 4	216 (86.7)	806 (72.9)
Stage 4s	0 (0)	54 (4.9)
Unknown	2 (0.8)	2 (0.2)
MYCN status, n (%)		
Amplified	68 (27.3)	NA
Not amplified	175 (70.3)	NA
Unknown	6 (2.4)	NA
Ploidy, n (%)		
Diploid (DI =1)	63 (25.3)	NA
Hyperdiploid (DI >1)	104 (41.8)	NA
Unknown	82 (32.9)	NA
Histology, n (%)		
Favorable	37 (14.9)	NA
Unfavorable	183 (73.5)	NA
Unknown	29 (11.6)	NA
Grade, n (%)		
Differentiating	13 (5.2)	NA
Undifferentiated or poorly differentiated	170 (68.3)	NA
Unknown	66 (26.5)	NA
MKI, n (%)		
High	52 (20.9)	NA
Intermediate	55 (22.1)	NA
Low	69 (27.7)	NA
Unknown	73 (29.3)	NA

NB, neuroblastoma; TARGET, Therapeutically Applicable Research to Generate Effective Treatments; ICGC, International Cancer Genome Consortium; NA, not applicable; INSS, International Neuroblastoma Staging System; MYCN, v-myc avian myelocytomatosis viral oncogene neuroblastoma derived homolog; DI, DNA index; MKI, mitosis-karyorrhexis index.

reporting checklist (available at https://tcr.amegroups.com/article/view/10.21037/tcr-24-269/rc).

Methods

Target dataset and clinical patient characteristics

The publicly available gene expression array of 249 NB patients that was updated to August 24, 2020 was accessed from the TARGET database (https://ocg.cancer.gov/programs/target/data-matrix). The available corresponding clinical data, including age, sex, *MYCN* status, and histology, of 249 patients diagnosed with NB by pathology were downloaded. The basic characteristics of the patients used in the survival analyses are shown in *Table 1*.

Then, the RNA-seq and clinical data of other 179 samples were downloaded from the International Cancer Genome Consortium (ICGC) up to November 26, 2019 (https://dcc.icgc.org/) to validate the model. The clinical characteristics consisted of sex, age and stage (*Table 1*).

Thus, the current research was exempt from local ethical review. The present study followed the TARGET data and ICGC data access policies and publication guidelines. This study was conducted in accordance with the Declaration of Helsinki (as revised in 2013).

Analysis of prognostic ferroptosis-related genes

In total, 259 ferroptosis-related genes were retrieved from the FerrDb Database (28) and are provided in Table S1. The DEGs were identified by the "limma" R package with a false discovery rate (FDR) <0.05. "ggplot2" and "ggrepel" were used to generate a volcano plot of DEGs. The heatmap generated by the "pheatmap" R package was used to describe the DEGs. Univariate Cox analysis was used to screen for prognostically relevant ferroptosis-related genes. The "Venn" package was used to detect and display the overlapping prognostic DEGs. The prognostic DEG results were entered to obtain processing functional annotation with gene lists using the "clusterProfiler" package to conduct Gene Ontology (GO) and Kyoto Encyclopedia of Genes and Genomes (KEGG) analyses based on the DEGs ($|\log2FC| \geq 1$, FDR <0.05). The heatmap was used to show the intersection of prognostic DEGs. Forest maps were used to generate the prognosis of DEGs. The protein-protein interactions (PPIs) of the intersecting genes were downloaded from the STRING database (29). The "igraph" and "reshape2" packages were used to visualize correction among prognostic DEGs.

Correlations between prognostic ferroptosis-related genes and drug responses

The patient tumors were implanted into immunodeficient rodents to develop the patient-derived xenograft (PDX) model, and PDX for Childhood Cancer Therapeutics (PCAT) is a resource of childhood cancer PDXs that provide genomic data and the correlation between genes and drug responses (30). The correlation between chemotherapy drugs used in NB patients, including cyclophosphamide, doxorubicin, carboplatin, and etoposide, and prognostic ferroptosis-related genes was analyzed by PCAT. Progressive disease (PD) was defined in this study as a >25% increase at the end of the study. Then, PD was further divided into PD1 and PD2 based on the tumor growth delay (TGD) value. If the TGD value was ≤1.5, the samples were defined as PD1; otherwise, they were considered PD2.

Development and validation of a prognostic ferroptosis-related gene model

The prognostic model was constructed by the least absolute shrinkage and selection operator (LASSO)-penalized Cox regression analysis using the "glmnet" package of R to shrink and choose variables further. Then, the risk score of patients was calculated according to the expression level of each gene and the corresponding Cox regression coefficient as follows: score = $e^{\text{sum (each gene's expression} \times \text{corresponding coefficient)}}$ (Table S2). Subsequently, based on the median risk score values, patients were stratified into high-risk (n=123) and low-risk (n=124) groups. To evaluate the prognostic model, tumor samples downloaded from ICGC were divided into low- (n=90) and high-risk (n=89) groups based on the median risk score. PCA and t-SNE using the "ggplot2" and "Rtsne" packages, respectively, were utilized to verify the distribution of different groups according to the expression of genes. The "survival" and "survminer" packages were used to analyze the survival between the high-risk and low-risk groups. The receiver operating characteristic (ROC) curves were plotted to assess the accuracy of the model with the "timeROC" R package.

Immune-related analysis

The single-sample gene set enrichment analysis (ssGSEA) was performed by the "limma", "ggpubr" and "reshape2" R packages to determine the infiltrating score of 16 immune cells and the activity of 13 immune-related pathways (table available at https://cdn.amegroups.cn/static/public/tcr-24-269-1.xlsx).

Statistical analysis

All figures in the present research were evaluated using R software (Version 4.2.0) and IBM SPSS 23.0. A two-tailed P<0.05 was considered statistically significant except for correlation analysis.

Results

Identification of prognostic ferroptosis-related DEGs (pFR-DEGs) in the target cohort

In total, 249 samples were downloaded from the TARGET Database. Then, two missing samples were deleted in the following study. From the FerrDb database, 259 ferroptosis-related genes were downloaded (28) and are provided in Table S1. Overall, 70 genes were identified as ferroptosis-related DEGs. *Figure 1A,1B* shows that 37/70 ferroptosis-related DEGs were upregulated in the COG high-risk group, while 33/70 were downregulated. Then, 13 ferroptosis-related genes were correlated with OS in the univariate Cox regression analysis. The pFR-DEGs were defined as the intersection of DEGs and prognostic ferroptosis-related genes. The five pFR-DEGs (*STEAP3*, *MAP1LC3A*, *ULK2*, *MTOR* and *TUBE1*) were considered crucial genes that play important roles in both NB and ferroptosis (all FDR <0.05, *Figure 2A-2C*, Table S2). The pairwise correlations among the pFR-DEGs are shown in *Figure 2D*. In addition, the PPI network and the correlation among these genes are visualized in *Figure 2E,2F*.

Functional enrichment analysis of pFR-DEGs

The intersection genes were then analyzed by KEGG pathway analyses and GO annotation to explore the pathways and biological functions, including biological processes (BP), cellular components (CC) and molecular functions (MF). The GO analysis results suggested that the genes were mainly enriched in late endosome, microtubule and vacuolar membrane. The biological processes shown in the results showed that autophagy and starvation response had significant relevance to pFR-DEGs, including "vacuole organization", "response to starvation", "macroautophagy", "response to nutrient levels", "response to extracellular

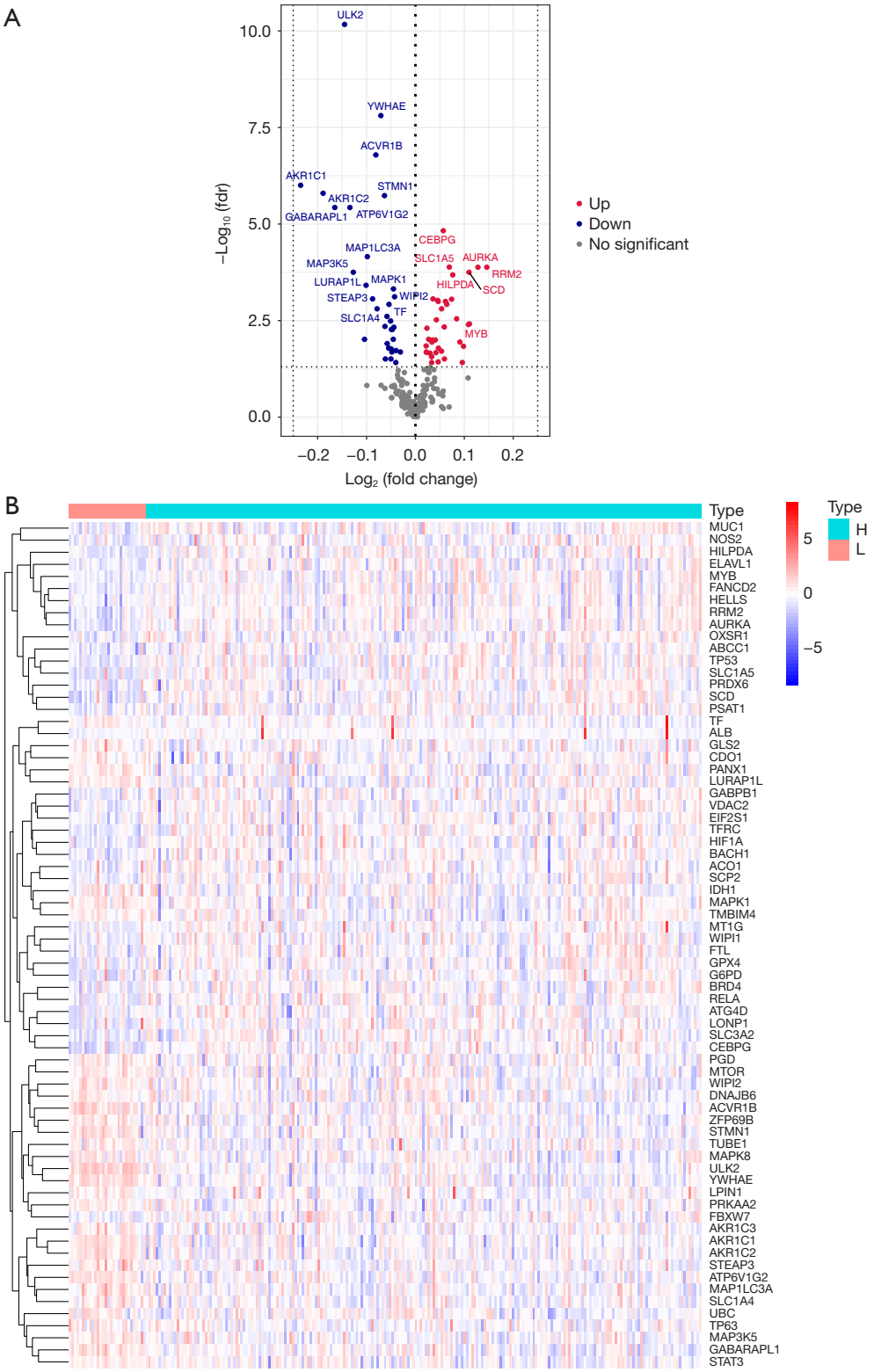

Figure 1 Differentially expressed ferroptosis-related genes. (A) Volcano plot of DEGs; the red dots indicate upregulated DEGs, the blue dots indicate downregulated DEGs, and the gray dots indicate no significant DEGs. (B) Heatmap of the expression profiles of 70 DEGs. H: high-risk group, L: low-risk group. DEGs, differentially expressed genes.

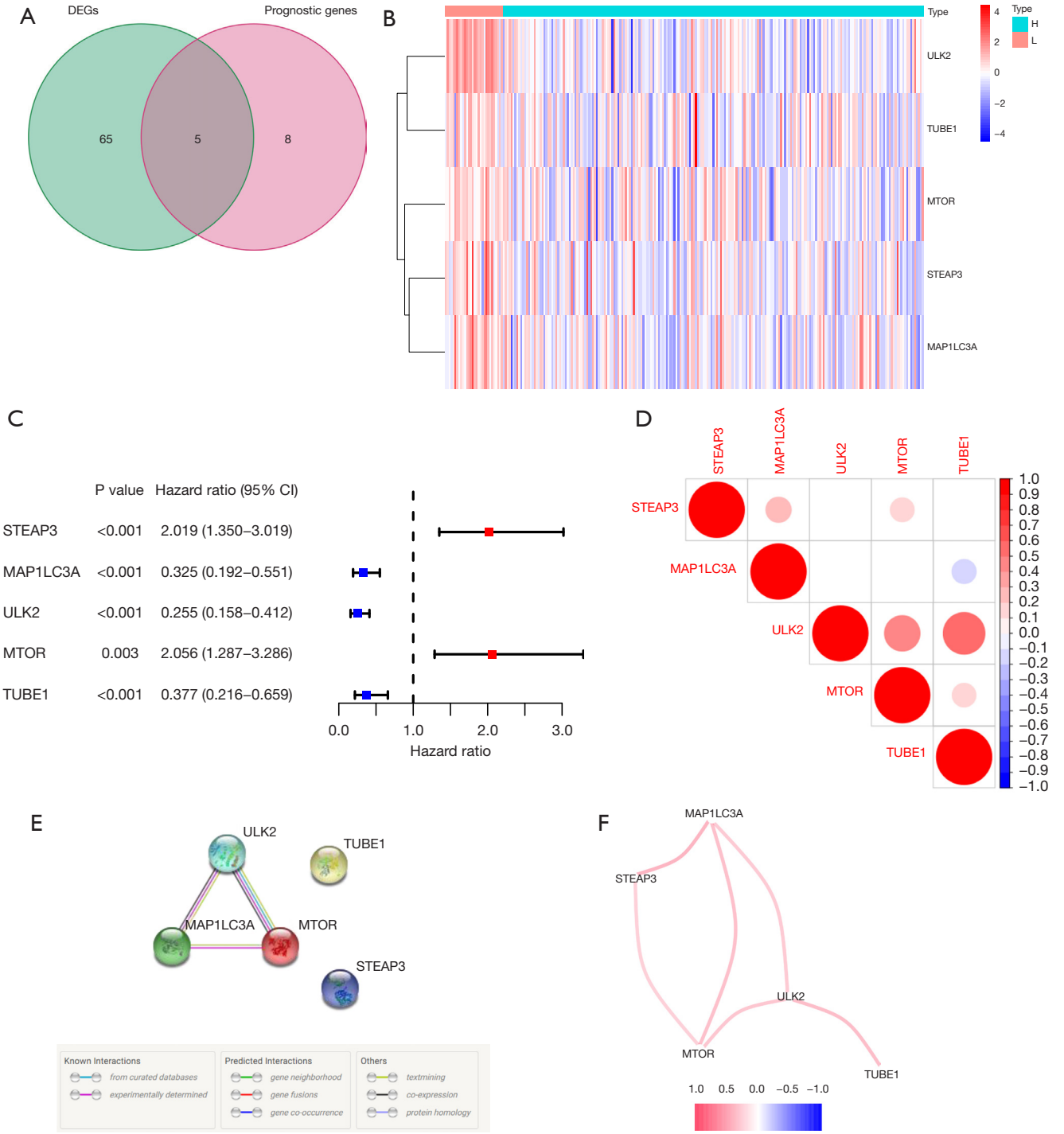

Figure 2 Identification of pFR-DEGs in the TARGET cohort. (A) Venn diagram displaying the overlapping prognostic DEGs. (B) Heatmap of pFR-DEGs; the red spectrum indicates high gene expression, and the blue spectrum indicates low gene expression. (C) Forest maps were used to generate the prognosis of pFR-DEGs. (D) The pairwise correlation among the pFR-DEGs. (E) The PPI network indicated the interactions among pFR-DEGs. (F) The correlation among pFR-DEGs; the different colors represent correlation coefficients. DEGs, differentially expressed genes; TARGET, Therapeutically Applicable Research to Generate Effective Treatments; pFR-DEGs, prognostic ferroptosis-related DEGs; PPI, protein-protein interaction; H: high-risk group, L: low-risk group.

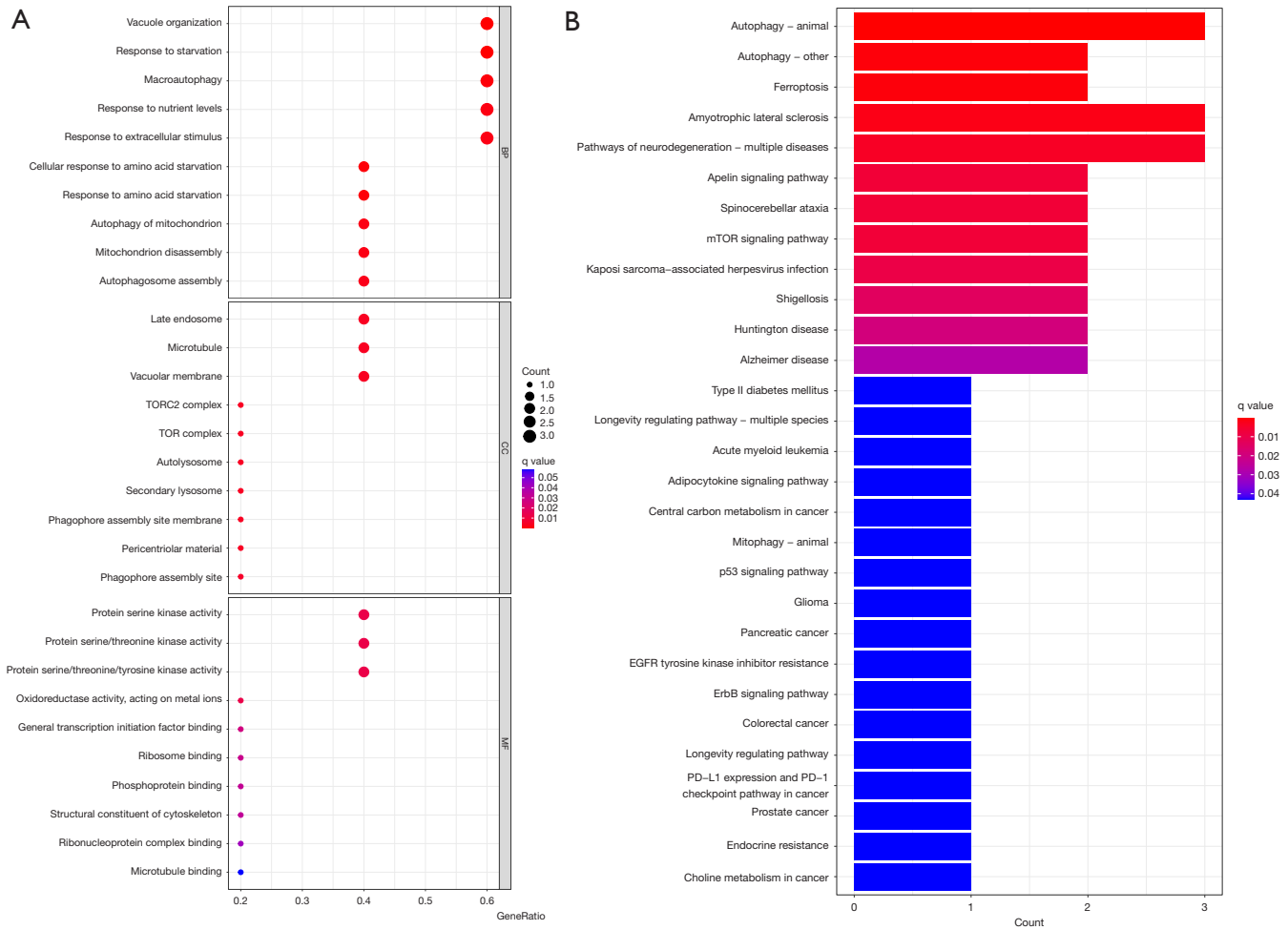

Figure 3 Functional enrichment analysis. (A) GO enrichment. (B) KEGG pathway analyses. GO, Gene Ontology; KEGG, Kyoto Encyclopedia of Genes and Genomes; BP, biological processes; CC, cellular components; MF, molecular functions; PD, progressive disease.

stimulus", "cellular response to amino acid starvation", "response to amino acid starvation", "autophagy of mitochondrion", and "mitochondrion disassembly and autophagosome assembly". In addition, the top 10 molecular functions were presented as follows: protein kinase activity, general transcription initiation factor binding and others (*Figure 3A*). Following enrichment analysis, the KEGG pathways revealed that the genes were significantly enriched in the "apelin signaling pathway", "*MTOR* signaling pathway", "adipocytokine signaling pathway", "p53 signaling pathway", "ErbB signaling pathway" and "PD-L1 expression and PD-1 checkpoint pathway in cancer" (*Figure 3B*).

Correlations between the pFR-DEGs and drug responses

Because the PCAT only included cyclophosphamide data, the drug response correlation analysis was performed among cyclophosphamide (CTX) and the 5 pFR-DEGs (*Figure 4*). As shown in *Figure 4A*, the median of the box plot produced by PD2 was 1.54, and the median of PD1 was 1.76. The box plot of *MAP1LC3A* indicated that the median values were 10.45 and 5.08 in PD1 and PD2, respectively (*Figure 4B*). In *Figure 4C*, the median *ULK2* expression in PD1 and PD2 was 7.33 and 5.06, respectively. Then, the median of the box plot produced by the PD1 algorithm was 10.85, and the median of PD2 was 7.38 in the *MTOR* gene (*Figure 4D*). Finally, the median of the box plot produced by the PD1

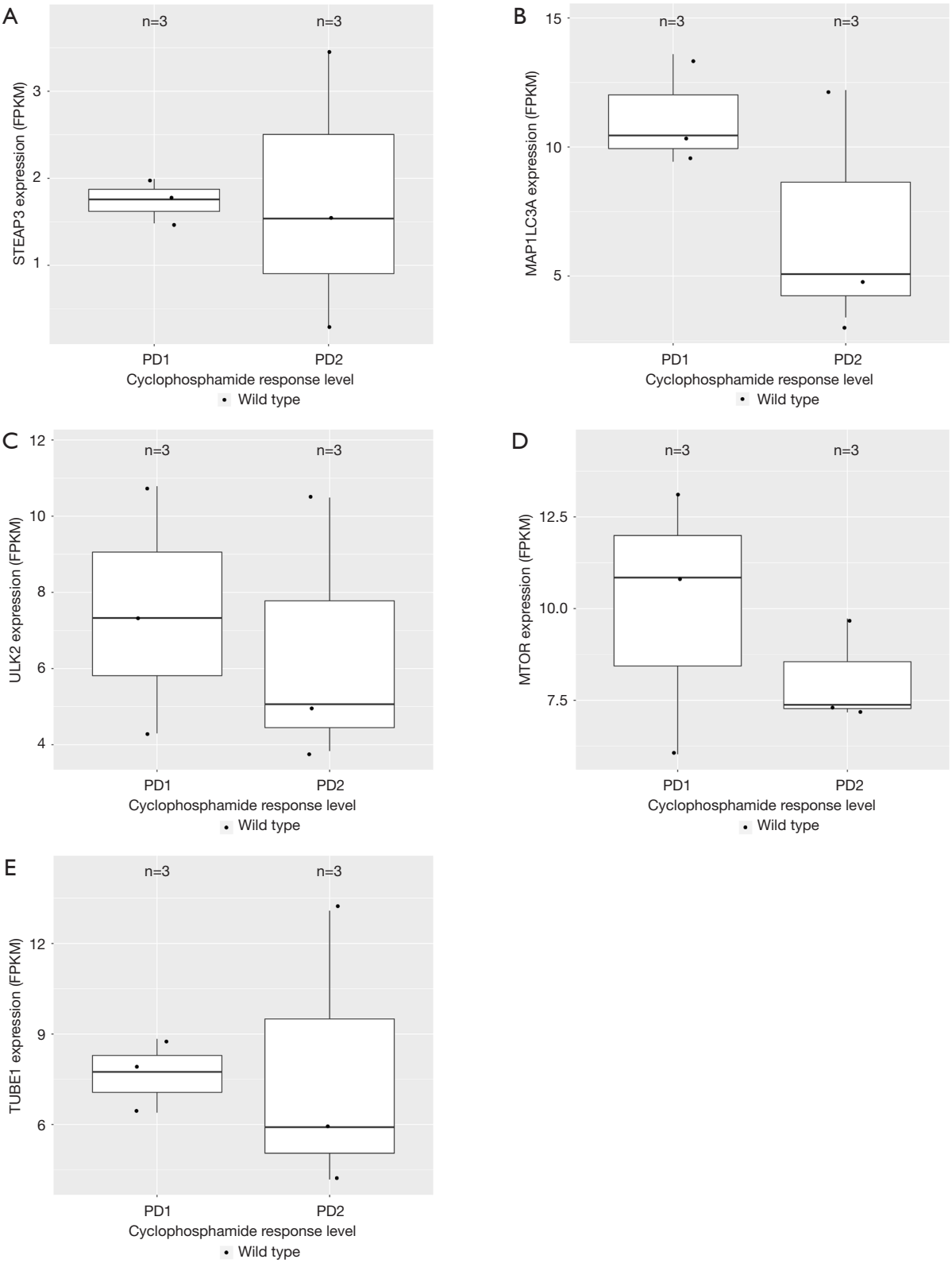

Figure 4 Correlations between DEGs and drug responses. CTX responses with *STEAP3* (A), *MAP1LC3A* (B), *ULK2* (C), *MTOR* (D) and *TUBE1* (E). DEGs, differentially expressed genes; CTX, cyclophosphamide; PD, progressive disease.

algorithm was 7.74, and the median of PD2 was 5.91 in the *TUBE1* gene (*Figure 4E*). Therefore, the box plot of PD1 in *MTOR* gene expression was in the highest position, which indicated that *MORT* expression is related to PD1 in NB patients compared with other pFR-DEGs. In addition, the interquartile range (IQR) of the *STEAP3* box plot generated by PD1 was 0.38, indicating the smallest discrete degree of expression in the drug response.

Establishment of a prognostic model

After LASSO regression analysis, a 5-gene signature was identified in the prognostic model, which is listed as follows: six-transmembrane epithelial antigen of the prostate 3 (*STEAP3*), microtubule associated protein 1 light chain 3 alpha (*MAP1LC3A*), unc-51 like autophagy activating kinase 2 (*ULK2*), mechanistic target of rapamycin (*MTOR*) and tubulin epsilon 1 (*TUBE1*) (Table S3). Then, patients were classified into high-risk (n=123) and low-risk (n=124) groups based on the median risk score (*Figure 5A*). In the prognostic model, the Kaplan-Meier curve indicated that the clinical outcome of patients in the high-risk group was inferior to that of patients in the low-risk group (*Figure 5B*, P<0.001). The areas under the curve (AUCs) for the 1-, 2- and 3-year survival rates were 0.672, 0.739 and 0.732, respectively, according to the time-dependent ROC curves (*Figure 5C*). Patients in the high-risk group had a higher probability of death earlier than those in the low-risk group, as shown in *Figure 5D*. The results of PCA and t-SNE analysis indicated that the patient distribution of the two different risk groups was located in two directions (*Figure 5E,5F*).

Independent prognostic value

The relationship between the risk model and clinical characteristics was tested by univariate and multivariate Cox regression to identify independent prognostic predictors. *MYCN* status, ploidy, histology and risk score were identified as significant risk factors in the univariate analysis (*Figure 6A*, all P<0.05). Then, the multivariate analysis demonstrated that histology [P=0.006, hazard ratio (HR) =4.446] and risk score (P=0.003, HR =1.933) were significant prognostic factors (*Figure 6B*).

Validation of the prognostic signature

The samples downloaded from ICGC were screened, and 179 samples were included in the validation, which were categorized into low-risk (n=90) and high-risk (n=89) groups based on the median risk score. The distribution of the two different risk groups is shown in *Figure 7A*, and the survival status of patients in the groups is shown in *Figure 7B*. Survival analysis of the validation model indicated that the patients in the high-risk group had a poorer prognosis (*Figure 7C*). The AUCs of the 5 related genes were 0.612, 0.669 and 0.640, respectively (*Figure 7D*). Finally, the results of PCA and t-SNE were similar to those of the prognostic model (*Figure 7E,7F*). The relationship between the risk score and clinical information was tested by univariate and multivariate Cox regression. Risk score was identified as significant risk factor in the univariate analysis (*Figure 8A*). Then, the multivariate analysis demonstrated that the risk score (P<0.001, HR =3.084) was a significant prognostic factor (*Figure 8B*).

Immune cell infiltration correlation analysis

To further explore the correlation between the model and immune microenvironment, ssGSEA was used to quantify the enrichment scores of different types of immune cells, associated pathways or functions. The results revealed that the high-risk group was related to more immune cells, such as interdigitating dendritic cells (iDCs), plasmacytoid dendritic cells (pDCs), T follicular helper cells (Tfhs) and T-helper 1 cells (Th1) (*Figure 9A*). Moreover, the scores of antigen presenting cell (APC) costimulation, CC chemokine receptor (CCR), checkpoint, T-cell coinhibition, T-cell costimulation and type I IFN response were significantly higher in the high-risk group (*Figure 9B*).

Discussion

Despite advances in NB therapy in recent years, high-risk NB patients still have a poor prognosis (31-33). Previous studies reported that Fth can induce ferroptosis cell death in NB, which provided new evidence for ferroptosis as a therapeutic target for NB (27). The current study is the first to construct a prognostic model related to ferroptosis genes in pediatric NB patients.

Ferroptosis, a type of regulated cell death driven by ROS, was discovered in 2012 (11,34-36). Ferroptosis has previously been associated with clinical outcomes in glioma, osteosarcoma, and breast cancer (37-39). The prognostic model consists of 5 ferroptosis-related genes (*STEAP3*, *MAP1LC3A*, *ULK2*, *MTOR* and *TUBE1*). STEAP3 plays

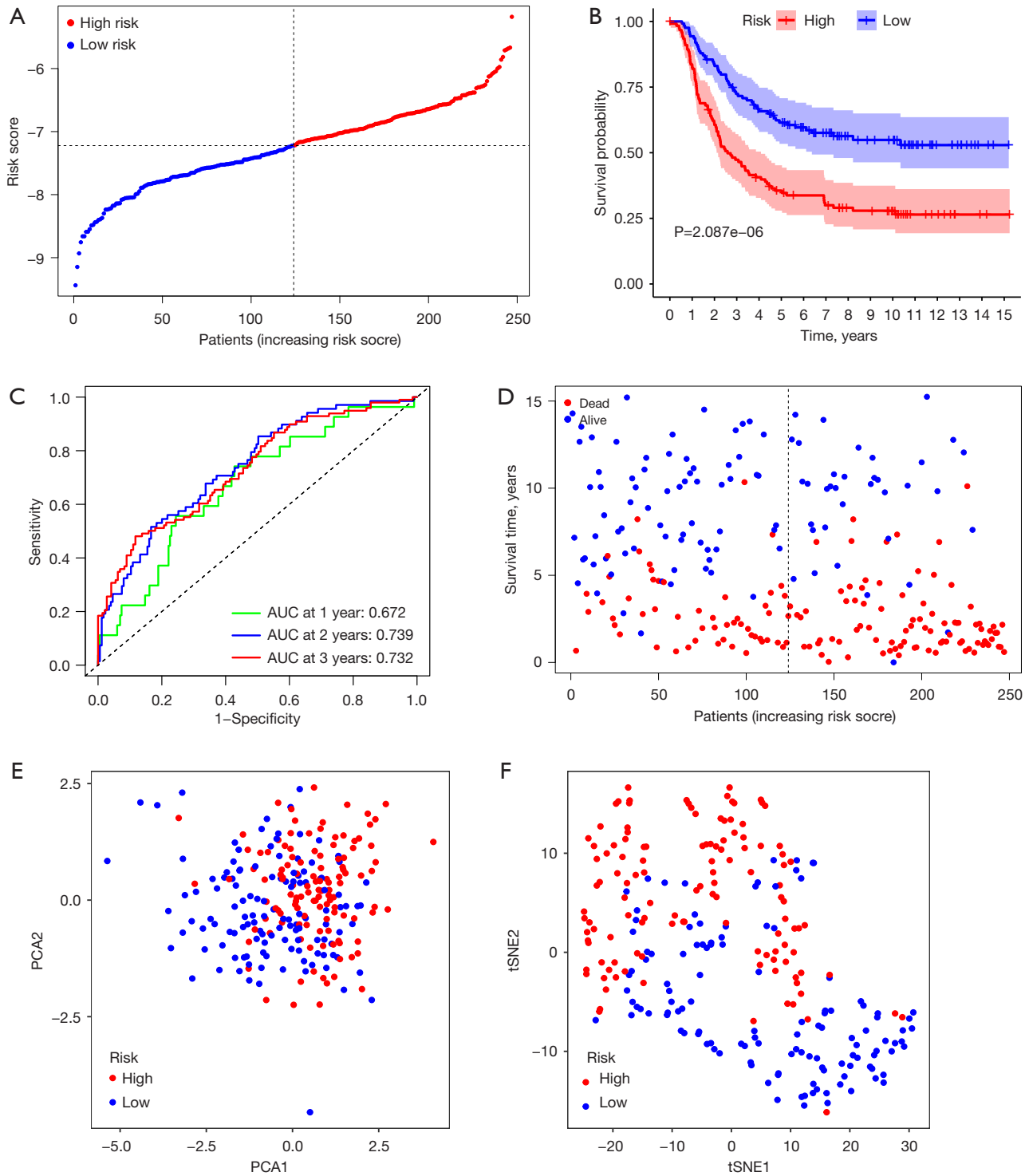

Figure 5 Prognostic analysis of the TARGET cohort. (A) The distribution and median value of the risk scores. (B) Kaplan-Meier curves of patients in the high-risk group and low-risk group. (C) Time-dependent ROC curves verified the predictive accuracy of the risk model. (D) The distributions of OS status, OS and risk scores. (E) PCA plot of the TARGET cohort. (F) t-SNE analysis of the TARGET cohort. TARGET, Therapeutically Applicable Research to Generate Effective Treatments; ROC, receiver operating characteristic; OS, overall survival; PCA, principal components analysis; t-SNE, t-distributed stochastic neighbor embedding.

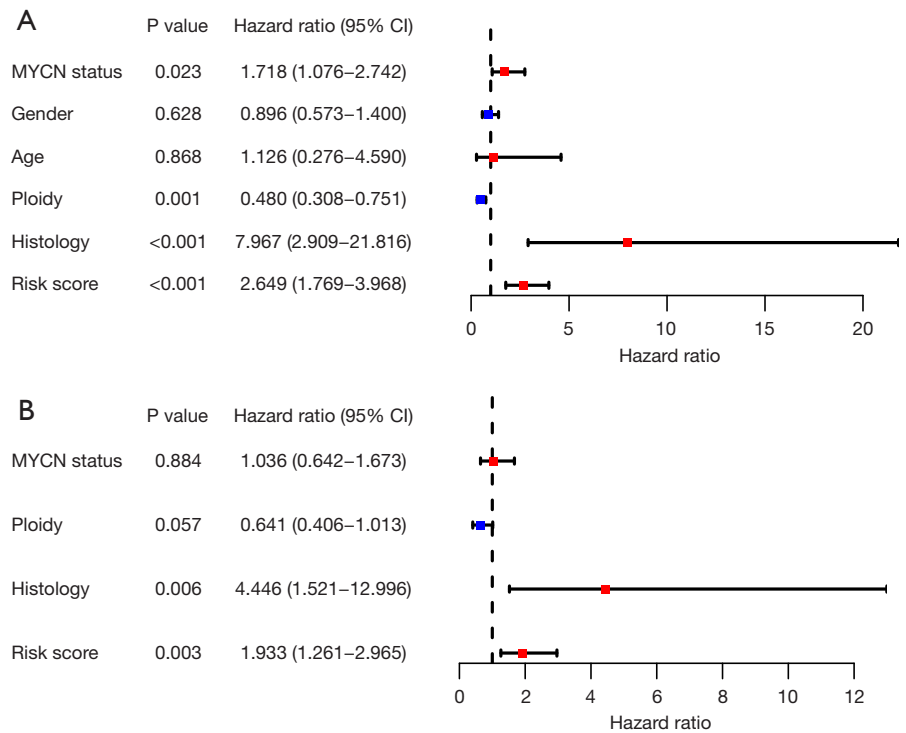

Figure 6 Independent prognostic value analysis in the TARGET cohort. (A) Univariate Cox regression analysis. (B) Multivariate Cox regression analysis. TARGET, Therapeutically Applicable Research to Generate Effective Treatments; MYCN, v-myc avian myelocytomatosis viral oncogene neuroblastoma derived homolog.

important in regulating iron metabolism (40). *MAP1LC3A* is part of LCS, which participates in the pathway of LC3-associated phagocytosis that is one function for autophagy protein (41-44). *ULK2* and *MTOR* are autophagy-related genes. As preview study, *ULK2* is an autophagy inducer gene, which was demonstrated that the overexpression of *ULK2* inhibited the glioma cell growth (45). And the *ULK* complexes can mediate *MTOR* signaling (46). *MTOR*, the mechanistic target of rapamycin, participates in cell growth and metabolism. Over the past decades, *MTOR* was found to play a central role in autophagy (47). The *TUBE1* gene is a member of the tubulin superfamily, which is important for microtubule triplet formation of centrioles (48,49). Ping *et al.* found that *TUBE1*, a prognostic ferroptosis-related gene, is significant in skin cutaneous melanoma (50). In the current study, *TUBE1* was proven as a prognostic ferroptosis-related gene in NB. All of the above genes are related to autophagy in ferroptosis. For the first time, they had been combined to describe the prognosis in NB patients. In the present study, we found that these genes were associated with poor prognosis in NB, but the process of them remains to be evaluated.

The five ferroptosis-related genes and their potential functions were analyzed by GO and KEGG enrichment analyses. The GO analyses in the subsequent study found that the cellular response plays an important role in biological processes, including response to starvation, response to nutrient levels, response to extracellular stimulus and response to amino acid starvation. Ni *et al.* demonstrated that ferroptosis was induced by the iron-starvation response (51). Similarly, some research noted that activating the iron-starvation response was important for the induction of ferroptosis (52). The molecular function of GO analyses showed that protein kinases are activated in ferroptosis, especially protein serine kinases. The protein serine kinase belonging to the mitogen-activated protein kinase family plays an important role in apoptosis (53). KEGG enrichment analyses identified some signaling pathways involved in ferroptosis in the present study. A previous study revealed that *p53* can regulate the ROS response and ferroptosis (54-56), and the signaling pathway of ferroptosis needs to be further elucidated.

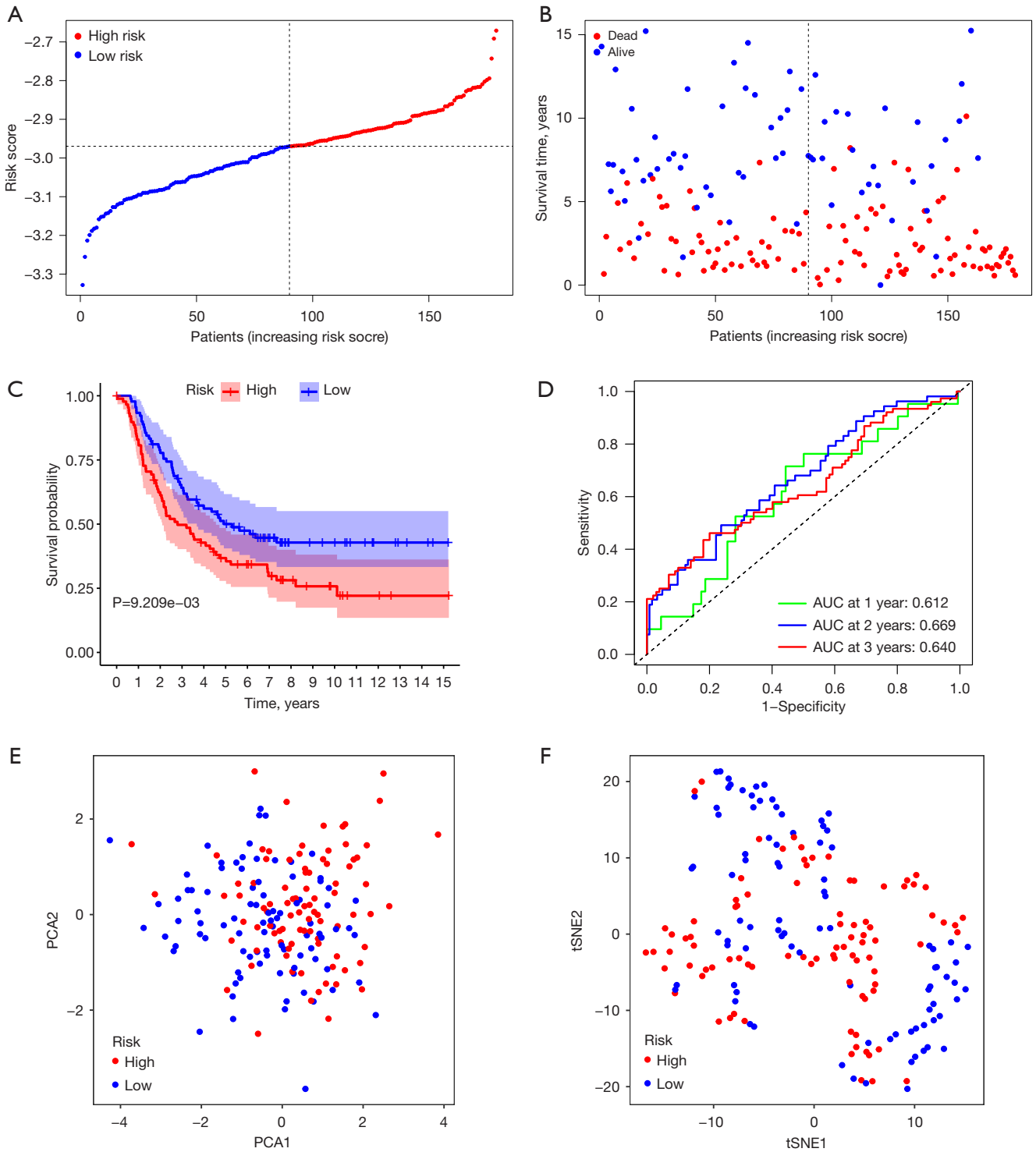

Figure 7 Validation of the prognostic signature in the ICGC cohort. (A) The distribution and median value of the risk scores. (B) The distributions of OS status, OS and risk scores. (C) Kaplan-Meier curves of patients in the high-risk group and low-risk group. (D) Time-dependent ROC curves verified the predictive accuracy of the risk model. (E,F) PCA plot and t-SNE analysis of the ICGC cohort, respectively. ICGC, International Cancer Genome Consortium; OS, overall survival; ROC, receiver operating characteristic; PCA, principal components analysis; t-SNE, t-distributed stochastic neighbor embedding.

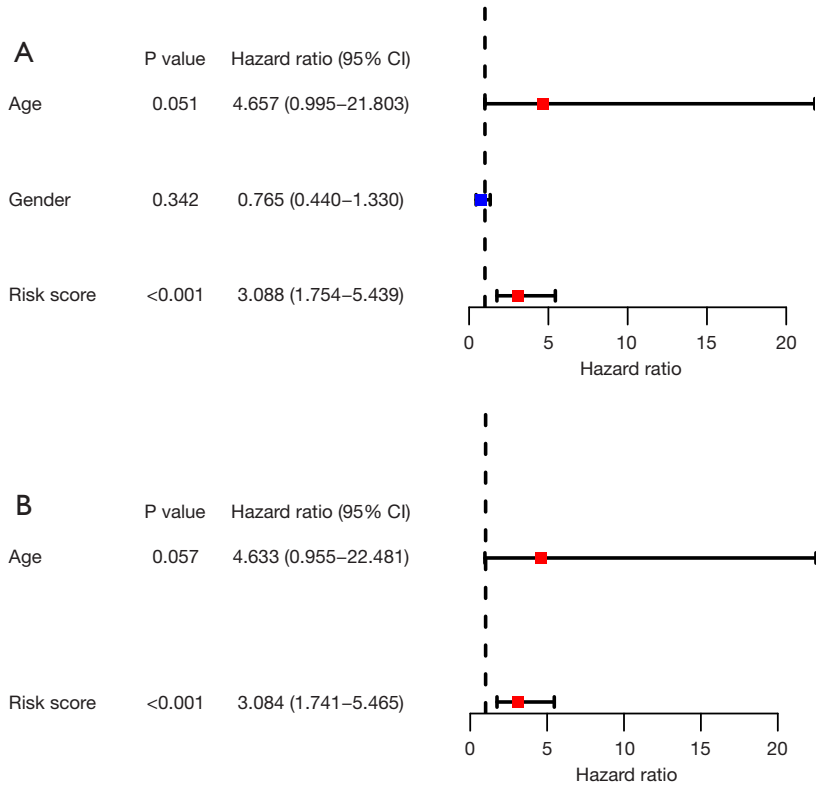

Figure 8 Independent prognostic value analysis in the ICGC cohort. (A) Univariate Cox regression analysis. (B) Multivariate Cox regression analysis. ICGC, International Cancer Genome Consortium.

Based on the correlation between pFR-DEGs and drug responses, we found that the expression of five related genes was different upon disease progression. Cyclophosphamide, an antitumor drug, induces ferroptosis by activating nuclear factor E2-related factor 2 (NRF2) and heme oxygenase-1 (HMOX-1) expression (57). There is little relevant research on CTX and ferroptosis. In our research, the expression of *MTOR* was highest in PD1, suggesting that the CTX response level of patients in PD1 might be correlated with *MTOR*, but the result requires further validation.

Many studies have focused on the prognosis of high-risk NB. The majority of familial NB is heritable in the *ALK* or *PHOX2B* gene mutation (58-61). Pugh *et al.* found that somatic mutations of genes are frequent by analyzing the genome, whole-exome and transcriptome sequencing of patients with high-risk NB (62). As in previous studies, the amplification of *MYCN* correlates with poor prognosis in high-risk disease (63). Many studies have been conducted on the prognosis of NB, but the genetic basis of NB remains largely unclear. The five genes identified for the prediction of patient survival were used to establish a new prognostic model. The good predictive performance of the model was demonstrated by Kaplan-Meier curves and AUC values. After dividing patients into high- and low-risk groups by the novel model, we used univariate and multivariate Cox regression to reevaluate the survival prognosis. The forest plot showed that prognostic indicators performed well in independent survival indicators, including histology and risk score. Therefore, the research data and method worked well, and the model could predict the prognostic value for NB patients.

Immune cell infiltration was explored between the high- and low-risk groups. The results showed that more immune cells were related to the high-risk group, including iDCs, pDCs, Tfh cells and Th1 cells. In recent years, immunotherapy has shown efficacy (64). A previous survey showed that pDCs have therapeutic potential for high-risk NB by activating the natural killer (NK) cell phenotype (65). Similarly, Mou *et al.* found that Tfh cells might promote the maturation of B cells and play an important role in the immune response in NB patients (66). Additionally, many studies have focused on immune function, such as APC

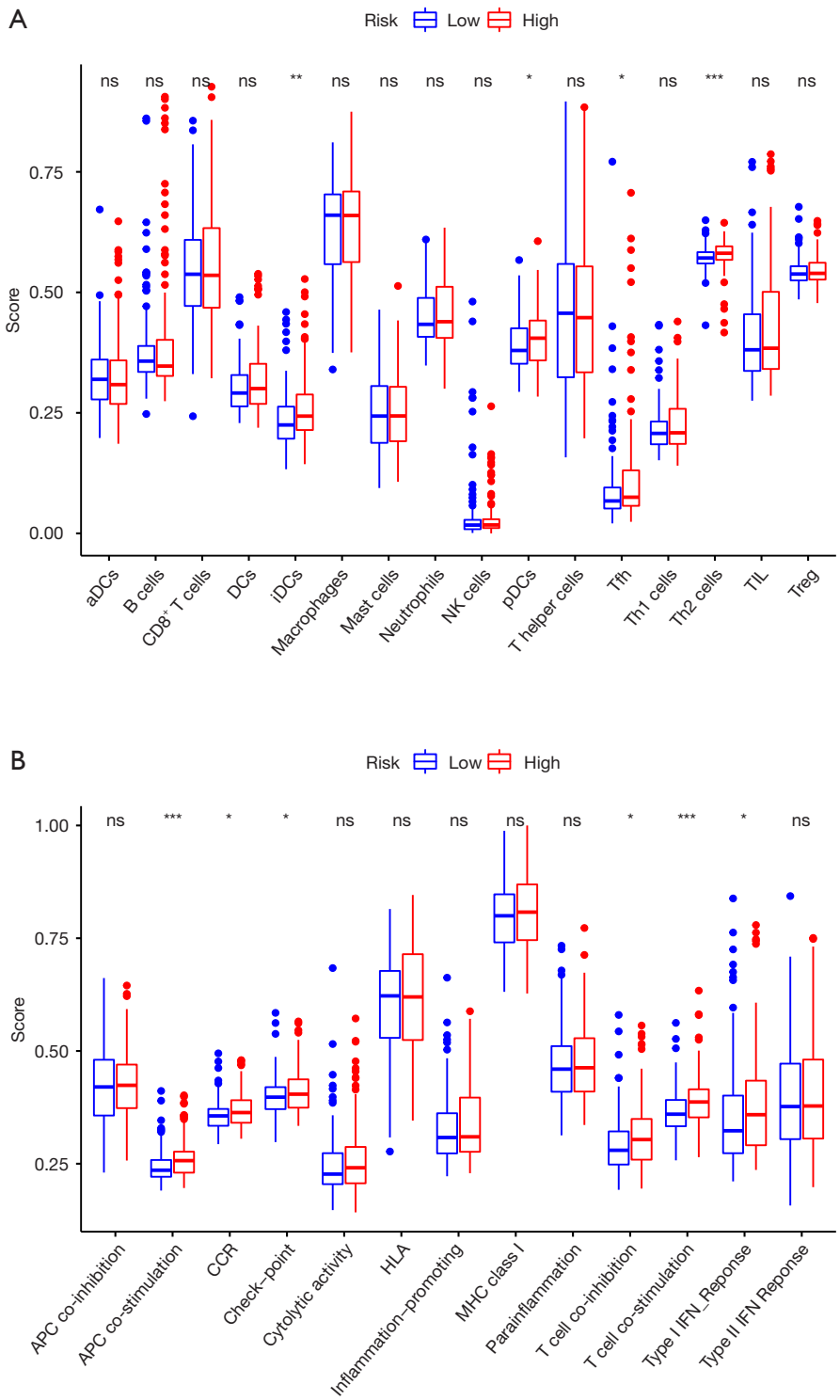

Figure 9 Comparison of ssGSEA scores between the high- and low-risk groups in TARGET. (A) The scores of 16 immune cells displayed in boxplots. (B) The scores of 13 immune-related functions shown in boxplots. Adjusted P values are shown as follows: ns, not significant. *, P<0.05, **, P<0.01, ***, P<0.001. ssGSEA, single-sample gene set enrichment analysis; TARGET, Therapeutically Applicable Research to Generate Effective Treatments.

costimulation, CCR, checkpoint, T-cell coinhibition, T-cell costimulation and the type I IFN response, which might provide potential immunotherapy for NB patients. The current survey established a ferroptosis-related prognostic model that might provide reliable information for NB patients. However, there are still some shortcomings in the present study. Retrospective data were used in our study, and further prospective experimental verification is needed. In addition, because of the small sample size, the HR of the model ranged widely in uni- and multivariate Cox regression. Lastly, due to the lack of clinical characteristics in ICGC data, the validation of independent prognostic value using ICGC data was weak. Hence, we will collect a clinical database and increase the sample size in future work.

Conclusions

In conclusion, the novel signature constructed by ferroptosis-related genes and the risk score model might be helpful for predicting prognosis and could improve immunotherapy.

Acknowledgments

Funding: None.

Footnote

Reporting Checklist: The authors have completed the TRIPOD reporting checklist. Available at https://tcr.amegroups.com/article/view/10.21037/tcr-24-269/rc

Peer Review File: Available at https://tcr.amegroups.com/article/view/10.21037/tcr-24-269/prf

Conflicts of Interest: All authors have completed the ICMJE uniform disclosure form (available at https://tcr.amegroups.com/article/view/10.21037/tcr-24-269/coif). The authors have no conflicts of interest to declare.

Ethical Statement: The authors are accountable for all aspects of the work in ensuring that questions related to the accuracy or integrity of any part of the work are appropriately investigated and resolved. The study was conducted in accordance with the Declaration of Helsinki (as revised in 2013).

References

1. Ward E, DeSantis C, Robbins A, et al. Childhood and adolescent cancer statistics, 2014. CA Cancer J Clin 2014;64:83-103.
2. Li X, Meng Y. A prognostic nomogram for neuroblastoma in children. PeerJ 2019;7:e7316.
3. Becker J, Wilting J. WNT signaling, the development of the sympathoadrenal-paraganglionic system and neuroblastoma. Cell Mol Life Sci 2018;75:1057-70.
4. Irwin MS, Naranjo A, Zhang FF, et al. Revised Neuroblastoma Risk Classification System: A Report From the Children's Oncology Group. J Clin Oncol 2021;39:3229-41.
5. Maris JM, Hogarty MD, Bagatell R, et al. Neuroblastoma. Lancet 2007;369:2106-20.
6. Mody R, Naranjo A, Van Ryn C, et al. Irinotecan-temozolomide with temsirolimus or dinutuximab in children with refractory or relapsed neuroblastoma (COG ANBL1221): an open-label, randomised, phase 2 trial. Lancet Oncol 2017;18:946-57.
7. Pinto NR, Applebaum MA, Volchenboum SL, et al. Advances in Risk Classification and Treatment Strategies for Neuroblastoma. J Clin Oncol 2015;33:3008-17.
8. Zhao H, Zhou X, Sun H, et al. Epigenome-wide association study reveals CpG sites related to COG of neuroblastoma. Biosci Rep 2020;40:BSR20200826.
9. Baker DL, Schmidt ML, Cohn SL, et al. Outcome after reduced chemotherapy for intermediate-risk neuroblastoma. N Engl J Med 2010;363:1313-23.
10. Liu KX, Naranjo A, Zhang FF, et al. Prospective Evaluation of Radiation Dose Escalation in Patients With High-Risk Neuroblastoma and Gross Residual Disease After Surgery: A Report From the Children's Oncology Group ANBL0532 Study. J Clin Oncol 2020;38:2741-52.
11. Dixon SJ, Lemberg KM, Lamprecht MR, et al. Ferroptosis: an iron-dependent form of nonapoptotic cell death. Cell 2012;149:1060-72.

12. Tang D, Chen X, Kang R, et al. Ferroptosis: molecular mechanisms and health implications. Cell Res 2021;31:107-25.
13. Stockwell BR, Friedmann Angeli JP, Bayir H, et al. Ferroptosis: A Regulated Cell Death Nexus Linking Metabolism, Redox Biology, and Disease. Cell 2017;171:273-85.
14. Nie J, Lin B, Zhou M, et al. Role of ferroptosis in hepatocellular carcinoma. J Cancer Res Clin Oncol 2018;144:2329-37.
15. Chen X, Li J, Kang R, et al. Ferroptosis: machinery and regulation. Autophagy 2021;17:2054-81.
16. Jiang X, Stockwell BR, Conrad M. Ferroptosis: mechanisms, biology and role in disease. Nat Rev Mol Cell Biol 2021;22:266-82.
17. Dixon SJ, Olzmann JA. The cell biology of ferroptosis. Nat Rev Mol Cell Biol 2024;25:424-42.
18. Chen X, Li X, Xu X, et al. Ferroptosis and cardiovascular disease: role of free radical-induced lipid peroxidation. Free Radic Res 2021;55:405-15.
19. Torti SV, Torti FM. Iron and cancer: more ore to be mined. Nat Rev Cancer 2013;13:342-55.
20. Ishimoto T, Nagano O, Yae T, et al. CD44 variant regulates redox status in cancer cells by stabilizing the xCT subunit of system xc(-) and thereby promotes tumor growth. Cancer Cell 2011;19:387-400.
21. Hasegawa M, Takahashi H, Rajabi H, et al. Functional interactions of the cystine/glutamate antiporter, CD44v and MUC1-C oncoprotein in triple-negative breast cancer cells. Oncotarget 2016;7:11756-69.
22. Hao S, Yu J, He W, et al. Cysteine Dioxygenase 1 Mediates Erastin-Induced Ferroptosis in Human Gastric Cancer Cells. Neoplasia 2017;19:1022-32.
23. Louandre C, Marcq I, Bouhlal H, et al. The retinoblastoma (Rb) protein regulates ferroptosis induced by sorafenib in human hepatocellular carcinoma cells. Cancer Lett 2015;356:971-7.
24. Eling N, Reuter L, Hazin J, et al. Identification of artesunate as a specific activator of ferroptosis in pancreatic cancer cells. Oncoscience 2015;2:517-32.
25. Hassannia B, Wiernicki B, Ingold I, et al. Nano-targeted induction of dual ferroptotic mechanisms eradicates high-risk neuroblastoma. J Clin Invest 2018;128:3341-55.
26. Geng N, Shi BJ, Li SL, et al. Knockdown of ferroportin accelerates erastin-induced ferroptosis in neuroblastoma cells. Eur Rev Med Pharmacol Sci 2018;22:3826-36.
27. Lu R, Jiang Y, Lai X, et al. A Shortage of FTH Induces ROS and Sensitizes RAS-Proficient Neuroblastoma N2A Cells to Ferroptosis. Int J Mol Sci 2021;22:8898.
28. Zhou N, Bao J. FerrDb: a manually curated resource for regulators and markers of ferroptosis and ferroptosis-disease associations. Database (Oxford) 2020;2020:baaa021.
29. Szklarczyk D, Franceschini A, Kuhn M, et al. The STRING database in 2011: functional interaction networks of proteins, globally integrated and scored. Nucleic Acids Res 2011;39:D561-8.
30. Yang J, Li Q, Noureen N, et al. PCAT: an integrated portal for genomic and preclinical testing data of pediatric cancer patient-derived xenograft models. Nucleic Acids Res 2021;49:D1321-7.
31. Moreno L, Barone G, DuBois SG, et al. Accelerating drug development for neuroblastoma: Summary of the Second Neuroblastoma Drug Development Strategy forum from Innovative Therapies for Children with Cancer and International Society of Paediatric Oncology Europe Neuroblastoma. Eur J Cancer 2020;136:52-68.
32. Park JR, Kreissman SG, London WB, et al. Effect of Tandem Autologous Stem Cell Transplant vs Single Transplant on Event-Free Survival in Patients With High-Risk Neuroblastoma: A Randomized Clinical Trial. JAMA 2019;322:746-55.
33. Ladenstein R, Pötschger U, Pearson ADJ, et al. Busulfan and melphalan versus carboplatin, etoposide, and melphalan as high-dose chemotherapy for high-risk neuroblastoma (HR-NBL1/SIOPEN): an international, randomised, multi-arm, open-label, phase 3 trial. Lancet Oncol 2017;18:500-14.
34. Li R, Yi X, Wei X, et al. EZH2 inhibits autophagic cell death of aortic vascular smooth muscle cells to affect aortic dissection. Cell Death Dis 2018;9:180.
35. Wei X, Yi X, Zhu XH, et al. Posttranslational Modifications in Ferroptosis. Oxid Med Cell Longev 2020;2020:8832043.
36. Galluzzi L, Vitale I, Aaronson SA, et al. Molecular mechanisms of cell death: recommendations of the Nomenclature Committee on Cell Death 2018. Cell Death Differ 2018;25:486-541.
37. Wan RJ, Peng W, Xia QX, et al. Ferroptosis-related gene signature predicts prognosis and immunotherapy in glioma. CNS Neurosci Ther 2021;27:973-86.
38. Lei T, Qian H, Lei P, et al. Ferroptosis-related gene signature associates with immunity and predicts prognosis accurately in patients with osteosarcoma. Cancer Sci 2021;112:4785-98.
39. Zhang K, Ping L, Du T, et al. A Ferroptosis-Related

lncRNAs Signature Predicts Prognosis and Immune Microenvironment for Breast Cancer. Front Mol Biosci 2021;8:678877.
40. Zhang F, Tao Y, Zhang Z, et al. Metalloreductase Steap3 coordinates the regulation of iron homeostasis and inflammatory responses. Haematologica 2012;97:1826-35.
41. Heckmann BL, Green DR. LC3-associated phagocytosis at a glance. J Cell Sci 2019;132:jcs222984.
42. Martinez J, Almendinger J, Oberst A, et al. Microtubule-associated protein 1 light chain 3 alpha (LC3)-associated phagocytosis is required for the efficient clearance of dead cells. Proc Natl Acad Sci U S A 2011;108:17396-401.
43. Sanjuan MA, Dillon CP, Tait SW, et al. Toll-like receptor signalling in macrophages links the autophagy pathway to phagocytosis. Nature 2007;450:1253-7.
44. Martinez J, Malireddi RK, Lu Q, et al. Molecular characterization of LC3-associated phagocytosis reveals distinct roles for Rubicon, NOX2 and autophagy proteins. Nat Cell Biol 2015;17:893-906.
45. Shukla S, Patric IR, Patil V, et al. Methylation silencing of ULK2, an autophagy gene, is essential for astrocyte transformation and tumor growth. J Biol Chem 2014;289:22306-18.
46. Jung CH, Jun CB, Ro SH, et al. ULK-Atg13-FIP200 complexes mediate mTOR signaling to the autophagy machinery. Mol Biol Cell 2009;20:1992-2003.
47. Saxton RA, Sabatini DM. mTOR Signaling in Growth, Metabolism, and Disease. Cell 2017;168:960-76.
48. Wang JT, Kong D, Hoerner CR, et al. Centriole triplet microtubules are required for stable centriole formation and inheritance in human cells. Elife 2017;6:e29061.
49. Atorino ES, Hata S, Funaya C, et al. CEP44 ensures the formation of bona fide centriole wall, a requirement for the centriole-to-centrosome conversion. Nat Commun 2020;11:903.
50. Ping S, Wang S, Zhao Y, et al. Identification and validation of a ferroptosis-related gene signature for predicting survival in skin cutaneous melanoma. Cancer Med 2022;11:3529-41.
51. Ni S, Yuan Y, Qian Z, et al. Hypoxia inhibits RANKL-induced ferritinophagy and protects osteoclasts from ferroptosis. Free Radic Biol Med 2021;169:271-82.
52. Alvarez SW, Possemato R. Leveraging the iron-starvation response to promote ferroptosis. Oncotarget 2018;9:10830-1.
53. Cross TG, Scheel-Toellner D, Henriquez NV, et al. Serine/threonine protein kinases and apoptosis. Exp Cell Res 2000;256:34-41.
54. Jiang L, Kon N, Li T, et al. Ferroptosis as a p53-mediated activity during tumour suppression. Nature 2015;520:57-62.
55. Kang R, Kroemer G, Tang D. The tumor suppressor protein p53 and the ferroptosis network. Free Radic Biol Med 2019;133:162-8.
56. Liu J, Zhang C, Wang J, et al. The Regulation of Ferroptosis by Tumor Suppressor p53 and its Pathway. Int J Mol Sci 2020;21:8387.
57. Shi H, Hou B, Li H, et al. Cyclophosphamide Induces the Ferroptosis of Tumor Cells Through Heme Oxygenase-1. Front Pharmacol 2022;13:839464.
58. Trochet D, Bourdeaut F, Janoueix-Lerosey I, et al. Germline mutations of the paired-like homeobox 2B (PHOX2B) gene in neuroblastoma. Am J Hum Genet 2004;74:761-4.
59. Janoueix-Lerosey I, Lequin D, Brugières L, et al. Somatic and germline activating mutations of the ALK kinase receptor in neuroblastoma. Nature 2008;455:967-70.
60. Mosse YP, Laudenslager M, Khazi D, et al. Germline PHOX2B mutation in hereditary neuroblastoma. Am J Hum Genet 2004;75:727-30.
61. Mossé YP, Laudenslager M, Longo L, et al. Identification of ALK as a major familial neuroblastoma predisposition gene. Nature 2008;455:930-5.
62. Pugh TJ, Morozova O, Attiyeh EF, et al. The genetic landscape of high-risk neuroblastoma. Nat Genet 2013;45:279-84.
63. Huang M, Weiss WA. Neuroblastoma and MYCN. Cold Spring Harb Perspect Med 2013;3:a014415.
64. Kholodenko IV, Kalinovsky DV, Doronin II, et al. Neuroblastoma Origin and Therapeutic Targets for Immunotherapy. J Immunol Res 2018;2018:7394268.
65. Cordeau M, Belounis A, Lelaidier M, et al. Efficient Killing of High Risk Neuroblastoma Using Natural Killer Cells Activated by Plasmacytoid Dendritic Cells. PLoS One 2016;11:e0164401.
66. Mou W, Han W, Ma X, et al. γδTFH cells promote B cell maturation and antibody production in neuroblastoma. BMC Immunol 2017;18:36.

Cite this article as: Lin X, Shao K, Lin Z, Liang Q, Li X, Chen H, Wu J. Identification of a ferroptosis-related gene signature for the prognosis of pediatric neuroblastoma. Transl Cancer Res 2024;13(7):3678-3694. doi: 10.21037/tcr-24-269

Table S1 Ferroptosis-related genes

ACSL4	*RB1*	*ATG7*	*GPT2*	*SLC2A8*
AKR1C1	*HSF1*	*ALOX12B*	*PSAT1*	*SLC2A12*
AKR1C2	*SQSTM1*	*ALOX15B*	*LURAP1L*	*GLUT13*
AKR1C3	*MUC1*	*ALOXE3*	*SLC7A5*	*SLC2A14*
ALOX15	*SLC3A2*	*G6PDX*	*HERPUD1*	*EIF2AK4*
ALOX5	*SLC40A1*	*ULK1*	*XBP1*	*TFAP2C*
ALOX12	*FTMT*	*ATG3*	*ZNF419*	*SP1*
ATP5MC3	*HSPA5*	*ATG4D*	*KLHL24*	*HBA1*
CARS1	*ATF4*	*BECN1*	*TRIB3*	*NNMT*
CBS	*HELLS*	*MAP1LC3A*	*ZFP69B*	*PLIN4*
CD44	*SCD*	*GABARAPL2*	*ATP6V1G2*	*HIC1*
CHAC1	*SRC*	*GABARAPL1*	*VEGFA*	*STMN1*
CISD1	*STAT3*	*ATG16L1*	*GDF15*	*RRM2*
CS	*PML*	*WIPI1*	*TUBE1*	*CAPG*
DPP4	*MTOR*	*WIPI2*	*ARRDC3*	*HNF4A*
FANCD2	*TP63*	*SNX4*	*CEBPG*	*NGB*
GCLC	*CDKN1A*	*ATG13*	*SNORA16A*	*YWHAE*
GLS2	*MIR137*	*ULK2*	*RGS4*	*GABPB1*
GPX4	*ENPP2*	*EGFR*	*BLOC1S5-TXNDC5*	*AURKA*
HSPB1	*FH*	*MAPK3*	*LOC390705*	*MIR4715*
LPCAT3	*CISD2*	*MAPK1*	*EIF2S1*	*RIPK1*
MT1G	*MIR9-1*	*BID*	*KIM-1*	*PRDX1*
NCOA4	*MIR9-2*	*CDKN2A*	*IL6*	*MIR30B*
PTGS2	*MIR9-3*	*SOCS1*	*CXCL2*	*SLC1A4*
RPL8	*ISCU*	*CDO1*	*RELA*	*PCK2*
SAT1	*OTUB1*	*MYB*	*HSD17B11*	*TXNIP*
SLC7A11	*LINC00336*	*MAPK8*	*AGPAT3*	*MIOX*
TFRC	*BRD4*	*MAPK9*	*SETD1B*	*TAZ*
TP53	*PRDX6*	*MAPK14*	*FTL*	*MTDH*
EMC2	*MIR17*	*LINC00472*	*MAFG*	*IDH1*
AIFM2	*SESN2*	*PRKAA2*	*IL33*	*SIRT1*
PHKG2	*NF2*	*PRKAA1*	*HAMP*	*FBXW7*
ACO1	*ARNTL*	*ELAVL1*	*DRD5*	*PANX1*
FTH1	*JUN*	*BAP1*	*DRD4*	*DNAJB6*
STEAP3	*CA9*	*MIR6852*	*MAP3K5*	*BACH1*
NFS1	*TMBIM4*	*ACVR1B*	*SLC2A1*	*LONP1*

Table S1 (*continued*)

https://dx.doi.org/10.21037/tcr-24-269

Table S1 (*continued*)

ACSL3	*PLIN2*	*TGFBR1*	*SLC2A3*	*VLDLR*
PEBP1	*MIR212*	*EPAS1*	*SLC2A6*	*TF*
ZEB1	*Fer1HCH*	*HILPDA*	*CAV1*	*TNFAIP3*
FADS2	*LAMP2*	*HIF1A*	*GCH1*	*TLR4*
NFE2L2	*ZFP36*	*IFNG*	*DUSP1*	*ATF3*
KEAP1	*PROM2*	*ANO6*	*NOS2*	*ATM*
NQO1	*CHMP5*	*LPIN1*	*NCF2*	*YY1AP1*
NOX1	*CHMP6*	*HMGB1*	*MT3*	*EGLN2*
ABCC1	*NOX5*	*LOC284561*	*UBC*	*TFR2*
SLC1A5	*DUOX1*	*ASNS*	*ALB*	*SLC38A1*
GOT1	*DUOX2*	*TSC22D3*	*TXNRD1*	*ATG5*
G6PD	*VDAC2*	*DDIT3*	*SRXN1*	*CYBB*
PGD	*PIK3CA*	*JDP2*	*GPX2*	*NOX3*
IREB2	*FLT3*	*SELENOS*	*BNIP3*	*NOX4*
HMOX1	*SCP2*	*ANGPTL7*	*OXSR1*	*KRAS*
ACSF2	*NRAS*	*DDIT4*	*HRAS*	

Table S2 The prognostic ferroptosis-related DEGs

STEAP3: six-transmembrane epithelial antigen of the prostate 3
MAP1LC3A: microtubule associated protein 1 light chain 3 alpha
ULK2: unc-51 like autophagy activating kinase 2
MTOR: mechanistic target of rapamycin
TUBE1: tubulin epsilon 1

DEGs, differentially expressed genes.

Table S3 Coefficient values of nine selected genes

Gene	Coef
STEAP3	0.792069519
MAP1LC3A	–1.220253731
ULK2	–0.613522324
MTOR	0.40441111
TUBE1	–0.347512278

https://dx.doi.org/10.21037/tcr-24-269